Electronic Supplementary Material (ESI) for Nanoscale.

Supporting Information

Large-Scale Synthesis of Uniform Lanthanide-Doped $NaREF_4$ Upconversion/Downshifting Nanoprobes for Bioapplications

Wenwu You, Datao Tu,* Wei Zheng, Xiaoying Shang, Xiaorong Song, Shanyong Zhou, Yan Liu, Renfu Li, and Xueyuan Chen*

Table S1 The volume of organic solvent for the synthesis of 1, 5, 20 and 200 mmol of Ln^{3+}-doped $NaREF_4$ NCs.

$NaREF_4$ (mmol)	1	5	20	200
OA + ODE (mL)	20	15	60	600
Solvent (mL):RE (mmol)	20	3	3	3

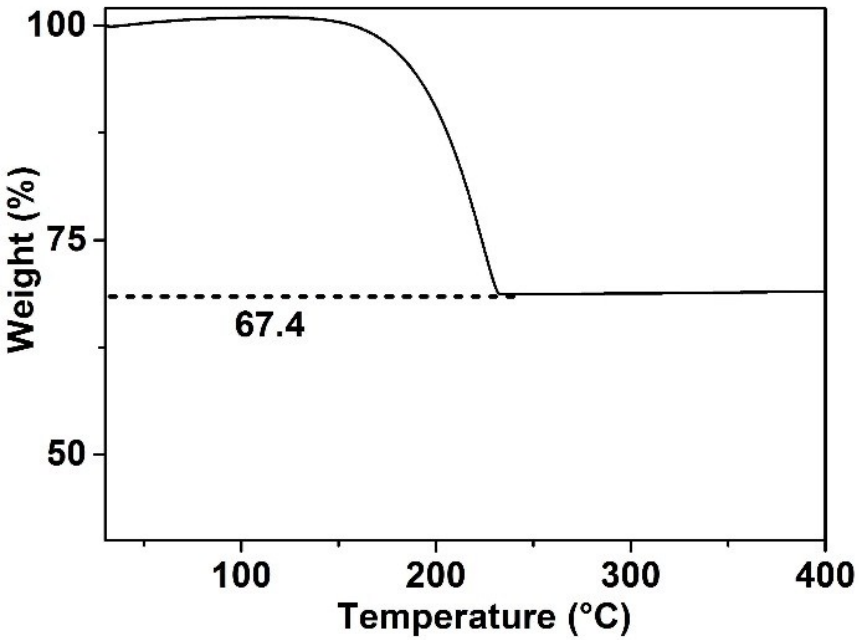

Fig. S1. TGA curve obtained by heating the $NaHF_2$ power under N_2 atmosphere in the temperature range of 30–400 °C at a rate of 10 °C/min. The $NaHF_2$ power started to decompose at 160 °C and completely decomposed at 235 °C. The weight losses were calculated to be 32.6%, which is consistent with the theoretical weight loss (~32.3%) resulting from the decomposition of $NaHF_2$ to NaF.

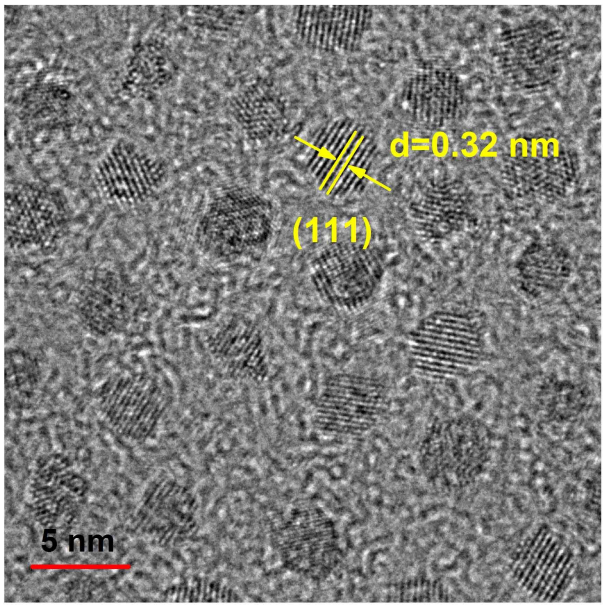

Fig. S2. High-resolution TEM (HRTEM) image of α-$NaGdF_4$:Yb,Er NCs. It displays clear lattice fringes with an observed d-spacing of 0.32 nm, which is in good agreement with the (111) plane of α-$NaGdF_4$, thus verifying the high crystallinity of the resulting NCs.

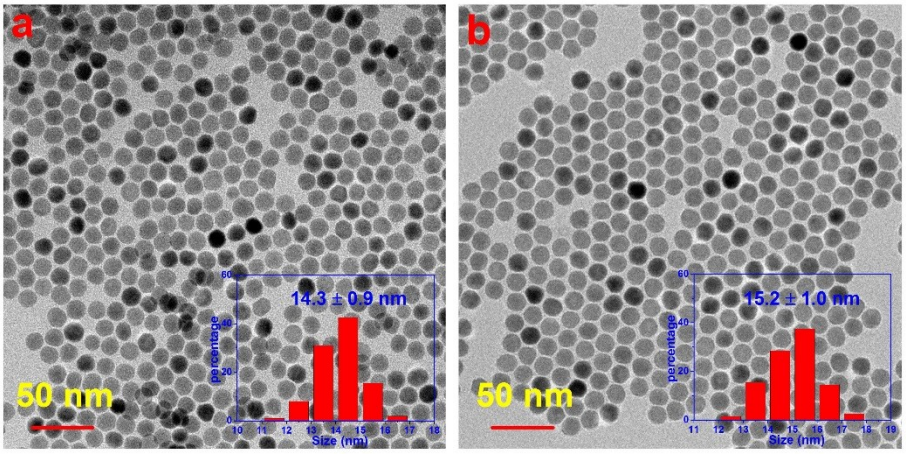

Fig. S3. TEM images of the β-$NaGdF_4$:Yb,Er NCs that were synthesized by **(a)** thermal co-decomposition (TCD) and **(b)** high temperature co-precipitation (HTCP) methods, respectively. Insets show their corresponding size distribution by randomly analyzing 200 particles.

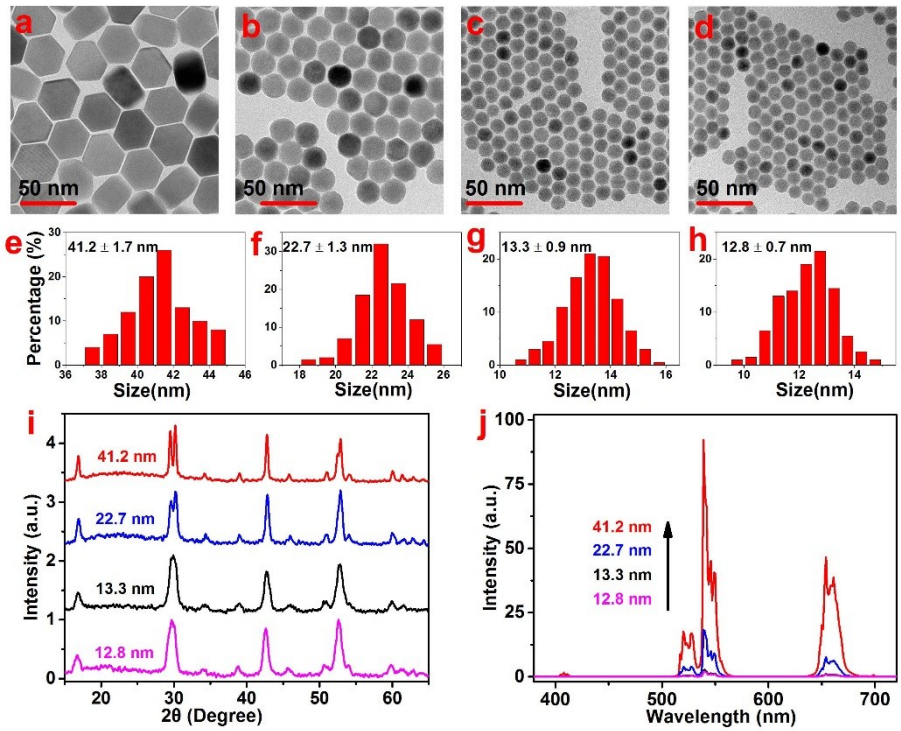

Fig. S4. (**a–d**) TEM images and (**e–h**) corresponding size distribution of the β-$NaGdF_4$:Yb,Er NCs, which were synthesized by addition of 0, 0.5, 1, and 1.5 mmol NaAc as sodium source in the reaction solution, respectively. It is observed that the size of final NCs decreased with the addition of NaAc. (**i**) Corresponding powder XRD pattern of (**a–d**). (**j**) UCL spectra of β-$NaGdF_4$:Yb,Er NCs of different size upon excitation at 980 nm. As the size of β-$NaGdF_4$:Yb,Er NCs increased from 12.8 to 41.2 nm, the UC intensity remarkably increased by ~50 times.

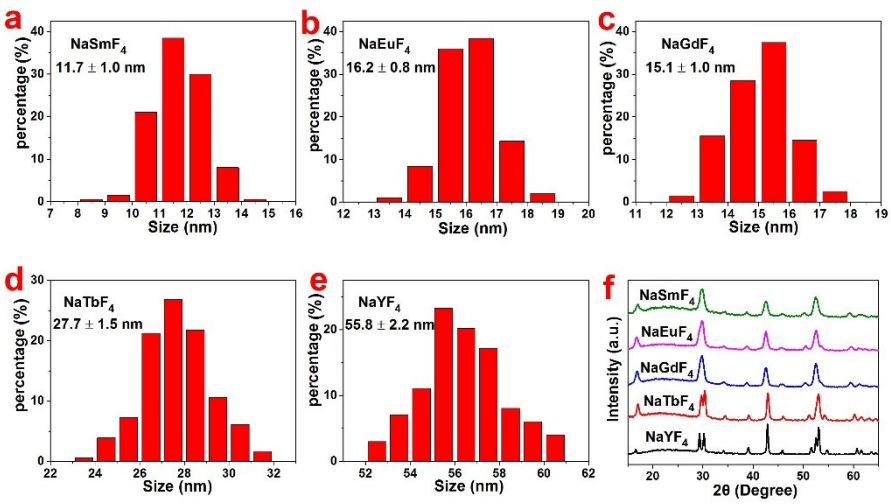

Fig. S5. Size distribution of the as-prepared (a) β-$NaSmF_4$, (b) β-$NaEuF_4$, (c) β-$NaGdF_4$, (d) β-$NaTbF_4$, and (e) β-$NaYF_4$ NCs. The narrow size variation (<10%) of all these samples confirms the well-controlled synthesis of the as-prepared β-$NaREF_4$ NCs. (**f**) Powder XRD pattern of the as-prepared β-phase $NaSmF_4$, $NaEuF_4$, $NaGdF_4$, $NaTbF_4$ and $NaYF_4$ NCs, respectively. All diffraction peaks can be well matched with the standard pattern of β-$NaREF_4$ and no other impurity peaks were detected, verifying the successful synthesis of pure β-$NaREF_4$ NCs.

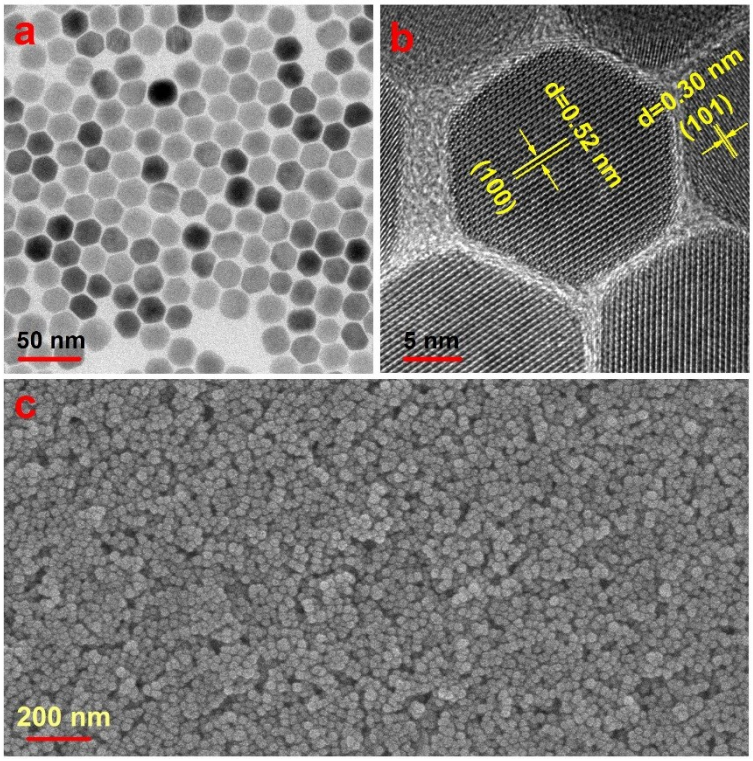

Fig. S6. Typical (**a**) TEM and (**b**) HRTEM images of the as-synthesized β-$NaGdF_4$:Yb,Er NCs (200 mmol). The lattice fringes can be clearly distinguished and the d-space between the lattice fringes were measured to be 0.52 and 0.30 nm, which are in good agreement with the lattice spacing of the (100) and (101) planes of β-$NaGdF_4$, respectively. (**c**) Typical SEM image of the as-synthesized β-$NaGdF_4$:Yb,Er NCs (200 mmol), which indicates their uniform size distribution.

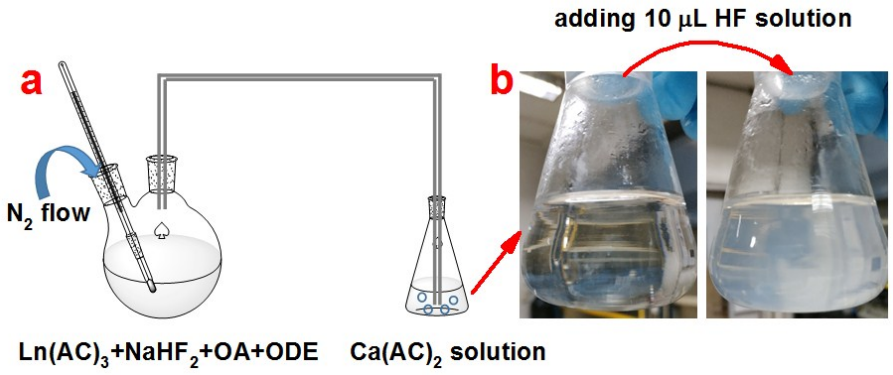

Fig. S7. (**a**) Scheme of the process of the proposed SLTD method, in which $Ca(Ac)_2$ solution was used for consuming the excessive HF during the synthesis of Ln^{3+}-doped $NaREF_4$ NCs. (**b**) Photographs of $Ca(Ac)_2$ solution after the synthesis of 20-mmol β-$NaGdF_4$:Yb,Er NCs (left). The $Ca(Ac)_2$ solution remained transparent after the reaction, which infers that the produced HF due to the decomposition of $NaHF_2$ has been essentially consumed for the nucleation and growth of Ln^{3+}-doped $NaREF_4$ NCs. However, turbid solution was observed after adding as low as 10 μL of HF solution into the $Ca(Ac)_2$ solution (right), owing to the formation of CaF_2 precipitations.

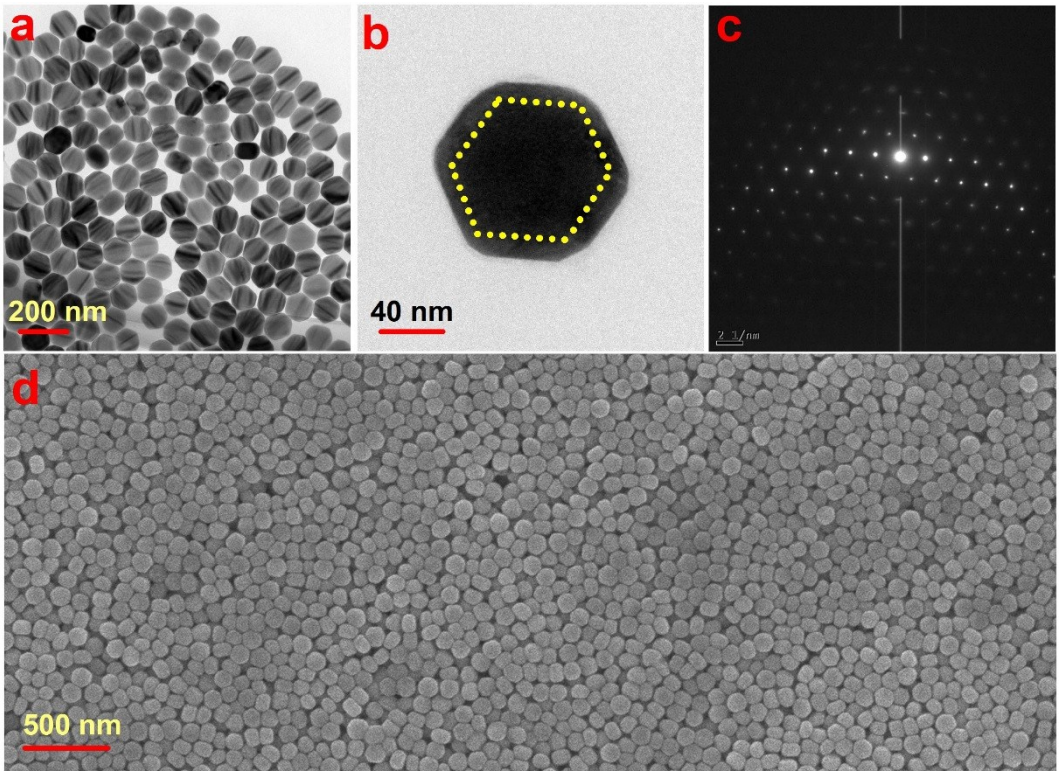

Fig. S8. (**a-b**) Typical TEM image of the synthesized β-$NaYF_4$:Yb,Er@$NaYF_4$ core/shell NCs (200 mmol) with the size of 110 ± 7.5 nm. The darker region in (**b**) corresponds to heavier ions (*i.e.*, Yb^{3+} and Er^{3+} ions) in the core and the brighter region corresponds to lighter ions (*i.e.*, Y^{3+} ions) in the shell. (**c**) Selected-area electron diffraction (SAED) pattern of β-$NaYF_4$:Yb,Er@$NaYF_4$ core/shell NCs in (**b**), indicative of the high crystallinity of the as-prepared core/shell NCs. (**d**) Typical SEM image of the as-prepared β-$NaYF_4$:Yb,Er@$NaYF_4$ core/shell NCs (200 mmol), which indicates their uniform size distribution.

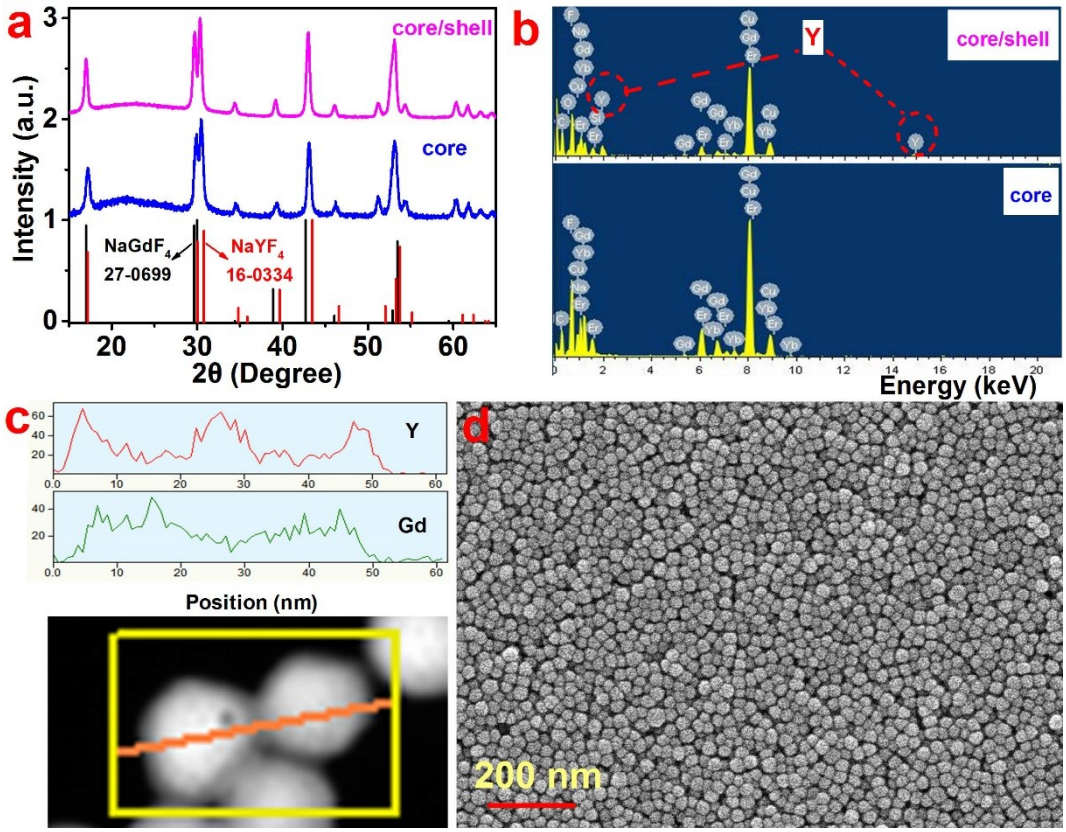

Fig. S9. (**a**) Powder XRD pattern of β-$NaGdF_4$:Yb,Er core and β-$NaGdF_4$:Yb,Er@$NaYF_4$ core/shell NCs (200 mmol). The black and red vertical lines represent the standard patterns of β-$NaGdF_4$ (JCPDS No. 27-0699) and β-$NaYF_4$ (JCPDS No. 16-0334), respectively. All diffraction peaks match well with the standard patterns of β-$NaREF_4$. (**b**) EDX spectroscopy analyses of β-$NaGdF_4$:Yb,Er core and β-$NaGdF_4$:Yb,Er@$NaYF_4$ core/shell NCs, which reveal the existence of Gd, Yb, Er, Na, F elements in β-$NaGdF_4$:Yb,Er core NCs and Gd, Yb, Er, Na, F, Y elements in the β-$NaGdF_4$:Yb,Er@$NaYF_4$ core/shell NCs. (**c**) Electron energy-loss spectroscopy (EELS) analysis conducted on two randomly selected core/shell NCs. It can be observed that Gd^{3+} ions were distributed in the inside region of the NCs while Y^{3+} ions were located in outside layer. (**d**) Typical SEM image of the synthesized β-$NaGdF_4$:Yb,Er@$NaYF_4$ core/shell NCs (200 mmol), which indicates their uniform size distribution.

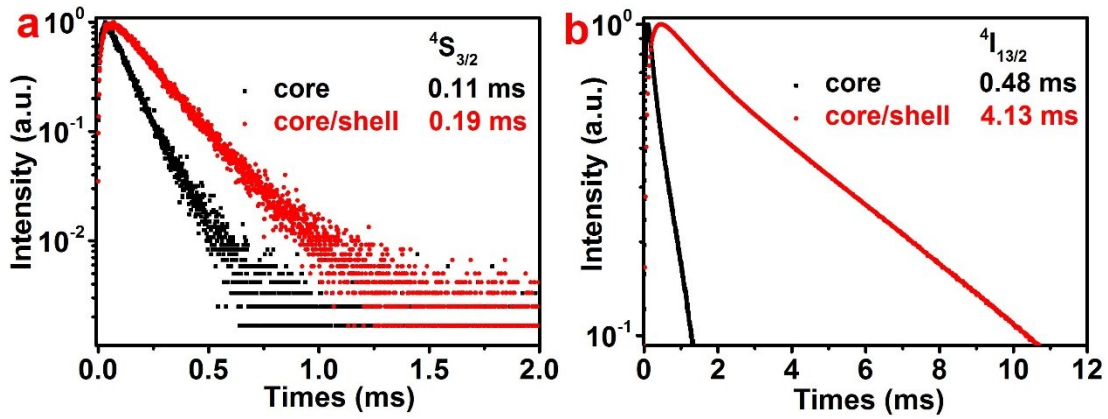

Fig. S10. (**a-b**) Photoluminescence (PL) decays from $^4S_{3/2}$ and $^4I_{13/2}$ of Er^{3+} in β-$NaGdF_4$:Yb,Er core and β-$NaGdF_4$:Yb,Er@$NaYF_4$ core/shell NCs upon excitation at 980 nm, respectively. After coating with the $NaYF_4$ shell, the PL lifetime of $^4S_{3/2}$ increased from 0.11 ms to 0.19 ms, and the PL lifetime of $^4I_{13/2}$ increased from 0.48 ms to 4.13 ms.

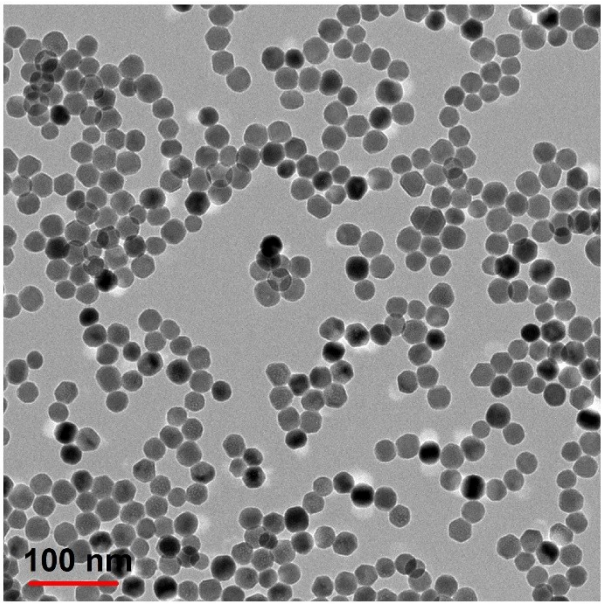

Fig. S11. Typical TEM image of the ligand-free β-$NaGdF_4$:Yb,Er@$NaYF_4$ NCs after acid treatment of the OA-capped NCs. It is observed that the ligand-free NCs exhibit good dispersibility and uniform size distribution.

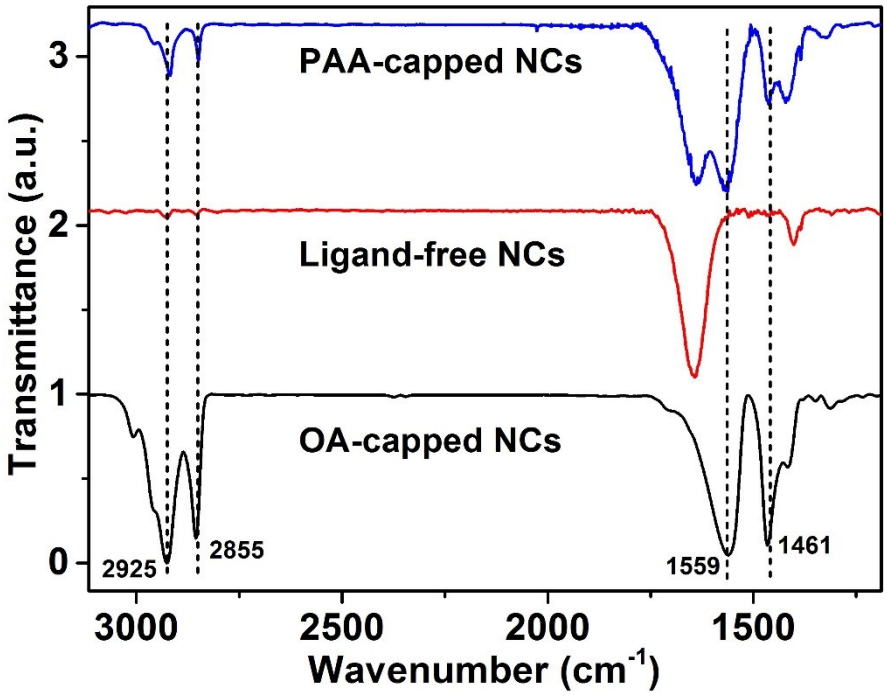

Fig. S12. FTIR spectra of the OA-capped, ligand-free and PAA-capped β-$NaGdF_4$:Yb,Er@$NaYF_4$ core/shell NCs. The original asymmetric and symmetric stretching vibrations of methylene (–CH_2–) in the long alkyl chain peaking at 2925 and 2855 cm^{-1} and the asymmetric and symmetric stretches of carboxyl (–COO–) peaking at 1559 and 1461 cm^{-1} disappear for the ligand-free NCs, indicating the successful removal of oleate ligands from the surface of OA-capped NCs. After PAA functionalization, the asymmetric and symmetric stretching vibrations of methylene (–CH_2–) in the long alkyl chain peaking at 2925 and 2855 cm^{-1} and the asymmetric and symmetric stretches of carboxyl (–COO–) peaking at 1559 and 1461 cm^{-1} appear, which indicates the successful capping of PAA on the surface of ligand-free NCs.

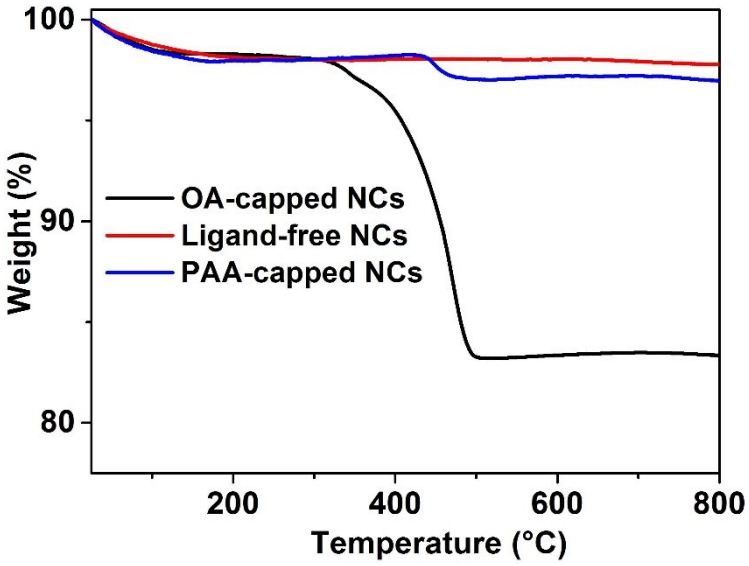

Fig. S13. TGA curves of the OA-capped, ligand-free, and PAA-capped $NaGdF_4$:Yb,Er@$NaYF_4$ NCs obtained by heating them under N_2 atmosphere in the temperature range of 30–800 °C at a rate of 10 °C/min. Different decomposition temperatures and weight losses were observed, due to the different ligands capping on the surface of NCs.

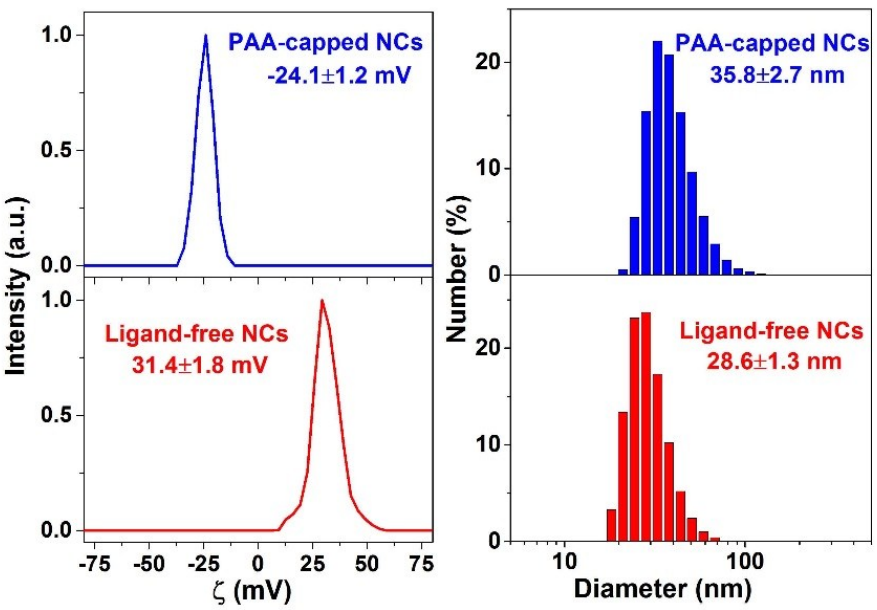

Fig. S14. Zeta potentials (left) and hydrodynamic diameter distribution (right) of the ligand-free and PAA capped β-$NaGdF_4$:Yb,Er@$NaYF_4$ core/shell NCs. The zeta potential of the ligand-free NCs is 31.4 mV, due to the positively-charged Ln^{3+} ions exposed on the surface of the NCs. After PAA functionalization, the zeta potential of the PAA-capped NCs changed from +31.4 to –24.1 mV. Meanwhile, the hydrodynamic diameter of the NCs increase from 28.6 nm to 35.8 nm.

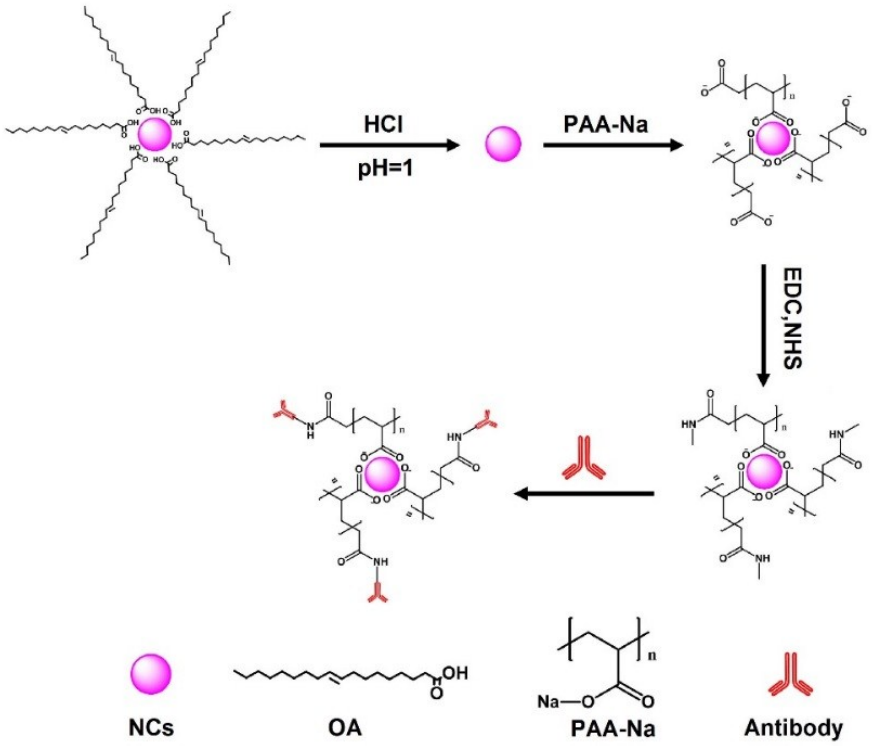

Fig. S15. Schematic illustration of the surface modification and antibody conjugation procedure. OA-capped NCs are washed with acid to yield ligand-free NCs. Thereafter, these hydrophilic NCs are modified with PAA by mixing the ligand-free NCs with PAA-Na in DI water. Finally, PSA antibodies are bioconjugated onto the PAA-capped NCs by the EDC/NHS coupling stragety.

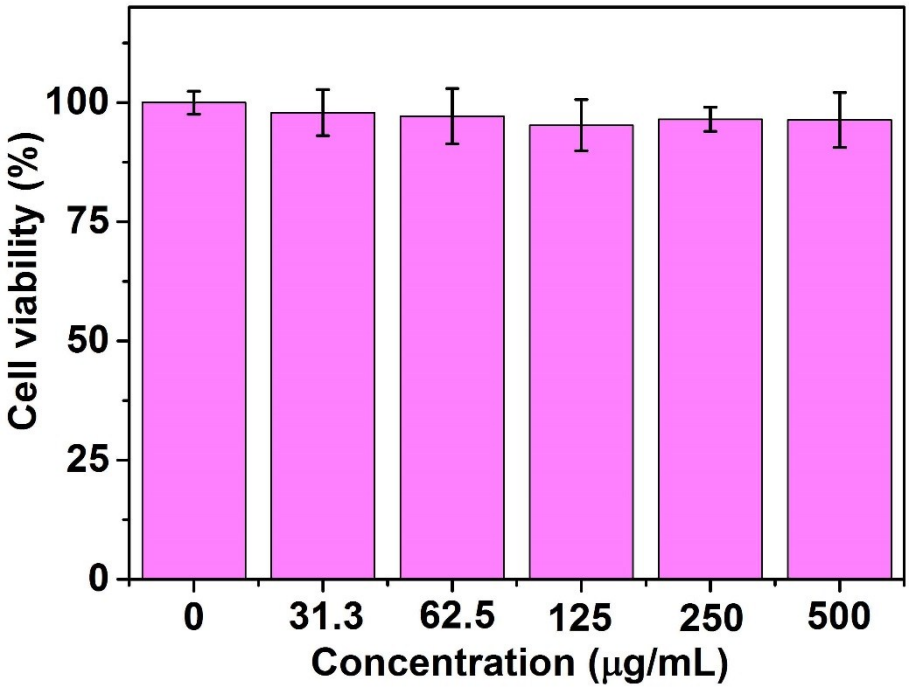

Fig. S16. In vitro cellular toxicity of DSPE-PEG-capped β-$NaGdF_4$:Yb,Er@$NaYF_4$ NCs towards HELF cells. The error bars represent standard errors (n = 3). The viability percentages of HELF cells were higher than 90% even when the concentration of the DSPE-PEG-capped β-$NaGdF_4$:Yb,Er@$NaYF_4$ NCs reached 500 μg mL^{-1}, which reveals the remarkably low cytotoxicity of the DSPE-PEG-capped β-$NaGdF_4$:Yb,Er@$NaYF_4$ NCs.